

# Study of the exotic $\Lambda_c^+$ with polarized photon beams

Qiang Zhao

Department of Physics, University of Surrey, Guildford, GU2 7XH, United Kingdom

We carry out an analysis of the pentaquark  $\Lambda_c^+$  photoproduction with polarized photon beams. Kinematical and dynamical aspects are examined for the purpose of determining  $\Lambda_c^+$ 's spin and parity. It shows that the polarized photon beam asymmetry in association with certain dynamical properties of the production mechanism would provide further information on its quantum numbers. Facilities at SP ring-8, JLab, ELSA, and ESRF will have access to them.

PACS numbers: 13.40.-f, 13.75.Jz, 13.88.+e

## I. INTRODUCTION

One of the major successes of the constituent quark model was its description of the established baryons as states consisting of three quarks, i.e., the minimal number of quarks to form a color-singlet "ordinary" baryon. Therefore, a baryon with strangeness  $S = +1$ , if it exists, can be regarded as "exotic". The newly-discovered  $\Lambda_c^+$  [1, 2, 3, 4, 5] seems to be the first experimental evidence for such a state. In particular, it has a quite low mass (1.54 GeV) and a narrow width  $< 25$  MeV, which certainly brings a strong impact on the conventional picture for the baryon structures.

Practically, the absence of the  $S = +1$  baryon in the three-quark picture will not rule out the quark model if an extra quark pair is present, e.g. uudds. The possible existence of such an object has been discussed before in the literature based on QCD phenomenology [6, 7].

On the other hand, a baryon with  $S = +1$  seems to be a natural output of the SU(3) Skyrme model, where the  $\Lambda_c^+$  is assigned to be a member of an exotic  $10$  multiplet of spin-parity  $1=2^+$  in company with the ordinary  $8$  and  $10$  multiplets [8]. Remarkably, the quantitative calculation [9] predicts that the  $S = +1$  member has a mass of 1.53 GeV with a narrow width of about 9 MeV, which is in good agreement with the experimental data. But is the  $\Lambda_c^+$  the Skyrme model predicted state?

In contrast to the Skyrme model predictions [8, 9], the quark model has a rather different picture for the exotic  $\Lambda_c^+$  due to possible quark flavor-spin correlations. For instance, if the lowest-mass pentaquark state is in a relative  $S$  wave, it will have spin-parity  $J^P = \frac{1}{2}^-$ . Therefore, to accommodate the  $\Lambda_c^+$  of  $1=2^+$  as predicted by the Skyrme model, asymmetric quark correlations seem likely. Stancu and Riska [10] have proposed a flavor-spin hyperfine interaction between light quarks, which is supposed to be strong enough to have the lowest state in the orbital  $P$  wave, and thus produces the quantum numbers  $1=2^+$  for the  $\Lambda_c^+$ . An alternative way to recognize the asymmetric quark correlations would be via clustered quark structures [11] as suggested by Jaffe and Wilczek [12] and Karliner and Lipkin [13]. To account for the narrow width of the  $\Lambda_c^+$ , Capstick, Page, and Roberts [14] have proposed that width suppression in  $\Lambda_c^+ \rightarrow \Lambda_c^0 \pi^+$  would be due to the isospin symmetry violating if the  $\Lambda_c^+$  is an isotensor state. However, the experimental analysis from SAPHIR [4] does not find signals for  $\Lambda_c^+ \rightarrow \Lambda_c^0 \pi^+$ . It thus presents a challenge for such an isospin-symmetry-violating solution. Nevertheless, even smaller widths for the  $\Lambda_c^+$  are claimed in the reports of Refs. [15, 16, 17, 18]. Carlson et al. [19] have shown the anti-decuplet  $10$  with  $J^P = \frac{1}{2}^-$  can lead to the same mass ordering  $10^- < 10^+ < 8^+$ , as in the Skyrme model. However, the question about the  $\Lambda_c^+$ 's narrow width has not been answered.

Apart from those efforts mentioned above, a large number of theoretical attempts have recently been devoted to understanding the nature of the  $\Lambda_c^+$ . Perspectives of the pentaquark properties and their consequences have been discussed in a series of activities in the Skyrme model [20, 21, 22, 23], quark models [24, 25, 26, 27, 28, 29, 30], and other phenomenologies [31, 32], which are essentially embedded on the phenomenological assumptions for the  $\Lambda_c^+$ 's quantum numbers, either to be a Skyrme  $10$  state of  $1=2^+$  or pentaquark of  $1=2^-, 1=2^+, 3=2^-, 3=2^+$ ; etc. QCD sum rule studies [33, 34, 35] and lattice QCD calculations [36, 37] are also reported. It is interesting to note that both QCD sum rules and lattice calculations are in favor of the  $\Lambda_c^+$  to be  $1=2^-$ . Note that the spin and parity of the  $\Lambda_c^+$  have not yet been unambiguously determined in experiment. This means that it is difficult to rule out any of those

possibilities. More essentially, such a situation also raises questions such as whether, or under what circumstances, there is any correspondence between the Skyrme and quark pictures. Or if the  $\Sigma^+$  is a pentaquark of  $1=2^+$ , since there must be angular momentum to overcome the intrinsic parity of uudds it implies there must be  $3=2^+$  partners. Then the questions could be how big the spin-orbit mass splitting between  $1=2^+$  and  $3=2^+$  would be, and which state was measured here [26, 38].

This situation eventually suggests that an explicit experimental confirmation of the quantum numbers of the  $\Sigma^+$  are not only essentially important for establishing the status of  $\Sigma^+$  on a fundamental basis [17, 39], but also important for any progress in understanding its nature, and the existence of its other partners [40]. A number of efforts to study the  $\Sigma^+$  in meson photoproduction and meson-nucleon scattering were made recently for such a purpose [41, 42, 43, 44, 45], where the  $\Sigma^+$  production in photonuclear reactions or  $\pi^-N$  scattering were estimated. The model calculations of the cross sections suggest a significant difference between  $1=2^+$  and  $1=2^-$ , which would certainly make sense for the attempt at determining the quantum numbers of  $\Sigma^+$ . This could be the first reference for distinguishing these two configurations, but should be taken with caution. The reason is that little knowledge about the  $\Sigma^+$  form factor is available and its total width still has large uncertainties. Nevertheless, the role played by other mechanism, e.g.,  $K$  exchange, is almost unknown, to which, however, the cross section is very sensitive. Due to such complexities, other observables should be measured, which will on the one hand provide more information for the  $\Sigma^+$ 's quantum numbers, and on the other hand provide constraints on theoretical phenomenologies.

In this work, we will study the photoproduction of  $\Sigma^+$  with polarized photon beams, and look for further information about the  $\Sigma^+$  which would be useful for the determination of its quantum numbers. First, in Sec. II we will examine the photon polarization transfer by studying the  $\Sigma^+$  decay in terms of its density matrix elements. In Sec. III, we will discuss the reaction mechanisms and analyze the polarized beam asymmetries in association with the differential cross section, for which different quantum numbers for  $\Sigma^+$  will lead to different features. Discussions and summaries will be given in Sec. IV.

## II. DENSITY MATRIX ELEMENTS FOR $\Sigma^+$ DECAY

The  $\Sigma^+$  is found to have a narrow width  $< 25$  MeV, which in principle makes the experimental access to its kinematic reconstruction easier than a broad state. In this sense, the production of  $\Sigma^+$  can be treated as a two-body reaction  $\gamma n \rightarrow K^+ \Sigma^+$ . This also gives access to the  $\Sigma^+$  production with polarized photon beams. Experimental efforts can be based on the present electromagnetic probes available at most of those experimental facilities, e.g., SP Ring-8, JLab, ELSA, and ESRF with their full-angle detectors. To be closely related to the experimental measurements and analyses, we will start with the experimentally measurable density matrix elements, which is useful for separating the kinematical information from the dynamical one, and look for signals which can help to pin down the quantum numbers of  $\Sigma^+$ .

Defining the z-axis as the photon momentum direction, and the reaction plane in x-z in the c.m. system of  $\gamma n$ , the transition amplitude for  $\gamma n \rightarrow K^+ \Sigma^+$  can be expressed as

$$T_{\lambda_N \lambda_{\Sigma^+}} = \langle \lambda_{\Sigma^+} | \hat{T} | \lambda_N \lambda_{\gamma} \rangle = \langle \lambda_{\Sigma^+} | \hat{T} | \lambda_N \lambda_{\gamma} \rangle = \langle \lambda_{\Sigma^+} | \hat{T} | \lambda_N \lambda_{\gamma} \rangle \quad (1)$$

where  $\lambda_{\gamma} = 1$ ,  $\lambda_N = 1/2$ ,  $\lambda_{\Sigma^+} = 0$ , and  $\lambda_{\Sigma^+}$  are helicities of photon, neutron,  $K^+$ , and  $\Sigma^+$ , respectively.

The decay of  $\Sigma^+$  into  $K^+ n$  is analyzed in the helicity frame, i.e. in the  $\Sigma^+$  rest frame; the azimuthal angles  $\phi$  and  $\phi'$  of  $K^+$  are defined with respect to the  $\Sigma^+$  three momentum  $\mathbf{P}_{\Sigma^+}$  in the  $\gamma n$  c.m. frame. The decay of  $\Sigma^+$  contains information for its spin and parity. The strategy here is to analyze three possible configurations for  $\Sigma^+$ , and compare their consequence in the  $K^+ n$  angular distributions with polarized photon beams.

The decay matrix can be written as  $\langle \lambda_n \lambda_{K^+} | \hat{T} | \lambda_{\Sigma^+} \rangle = \langle \lambda_n \lambda_{K^+} | \hat{T} | \lambda_{\Sigma^+} \rangle$ ; where  $\hat{T}$  denotes the strong transition operator. For the  $\Sigma^+$  of  $1=2^-$ ,  $1=2^+$ , and  $3=2^+$ , we apply the following effective Lagrangians to derive the transition operators:

$$\begin{aligned} L_{\text{eff}}(1=2^-) &= g_{NK} \bar{N} \gamma_5 \gamma_\mu K \partial_\mu \Sigma + \text{H.c.}; \\ L_{\text{eff}}(1=2^+) &= g_{NK} \bar{N} \gamma_\mu K \partial_\mu \Sigma + \text{H.c.}; \\ L_{\text{eff}}(3=2^+) &= g_{NK} \bar{N} \gamma_\mu \gamma_5 K \partial_\mu \Sigma + \text{H.c.}; \end{aligned} \quad (2)$$

where  $\bar{N}$ ,  $N$  and  $K$  denote the field of  $\Sigma^+$ , neutron and  $K^+$ , respectively. The nonrelativistic expansion in the  $\Sigma^+$  rest frame ( $\mathbf{P}_{\Sigma^+} = 0$ ) gives:

$$\begin{aligned} \hat{T}^{(s;1=2^-)} &= C; \\ \hat{T}^{(p;1=2^+)} &= C \frac{\mathbf{p} \cdot \mathbf{p}'}{p}; \\ \hat{T}^{(p;3=2^+)} &= CS \frac{\mathbf{p} \cdot \mathbf{p}'}{p}; \end{aligned} \quad (3)$$

where  $C$  is a spin and angular independent factor, and  $p^0$  is the three momentum carried by  $K^+$  in the  $^+$  rest frame. Note that  $L_{\text{eff}} (l=2)$  is different from the treatment of Ref. [43], where the effective Lagrangian is obtained by removing the  $s$  matrix from the pseudovector/pseudoscalar coupling, though the  $S$ -wave decay leads to the same form for the transition operator.

$$A. \quad ^+ \text{ of } l=2^+$$

Starting with the  $l=2^+$  configuration, the decay transition can be expressed as

$$\begin{aligned} \hat{R}_{s_f; s}^{\dagger} \ln; s_f; P \quad p^0 \hat{f}^{(p; l=2^+)} j^+; s; P = 0 i \\ = C \sqrt{2} D_{00}^1(\theta; \phi; \psi)_{s_f; s} \quad p^0 \sqrt{2} D_{10}^1(\theta; \phi; \psi)_{s_f; s-1} + p^0 \sqrt{2} D_{10}^1(\theta; \phi; \psi)_{s_f; s+1}; \end{aligned} \quad (4)$$

where we use the short-hand symbol  $\hat{R}_{s_f; s}$  to denote the transition elements and  $D_{MN}^1(\theta; \phi; \psi)$  is the Wigner rotation function with the convention of Ref. [46]. Namely,  $D_{MN}^I(\theta; \phi; \psi) = d_{MN}^I(\phi) e^{i(M\theta + N\psi)}$ . Under this convention, those rotation functions will be

$$\begin{aligned} D_{00}^1(\theta; \phi; \psi) &= d_{00}^1(\theta) = \cos \theta; \\ D_{10}^1(\theta; \phi; \psi) &= d_{10}^1(\theta) e^{i\phi} = \frac{\sin \theta}{2} e^{i\phi}; \\ D_{10}^1(\theta; \phi; \psi) &= d_{10}^1(\theta) e^{i\psi} = \frac{\sin \theta}{2} e^{i\psi}; \end{aligned} \quad (5)$$

The angular distribution of  $^+ \rightarrow K^+ \pi$  can be then described by the density matrix elements  $\rho_{s; s^0} (^+)$ :

$$\begin{aligned} W(\theta; \phi; \psi) &= \sum_{s_f; s_f^0; s; s^0} \hat{R}_{s_f; s}^{\dagger} \rho_{s; s^0} (^+) \hat{R}_{s_f^0; s^0} \\ &= \sum_{s; s^0} \hat{R}_{\frac{1}{2}; s}^{\dagger} \rho_{s; s^0} \hat{R}_{\frac{1}{2}; s^0} + \hat{R}_{\frac{1}{2}; s}^{\dagger} \rho_{s; s^0} \hat{R}_{\frac{1}{2}; s^0} \\ &\quad + \hat{R}_{\frac{1}{2}; s}^{\dagger} \rho_{s; s^0} \hat{R}_{\frac{1}{2}; s^0} + \hat{R}_{\frac{1}{2}; s}^{\dagger} \rho_{s; s^0} \hat{R}_{\frac{1}{2}; s^0}; \end{aligned} \quad (6)$$

Substituting Eq. (4) into the above, and after some simple algebra, we arrive at

$$\begin{aligned} W(\theta; \phi; \psi) &= [1 - \sin^2 \theta \cos^2 \psi]_{\frac{1}{2}; \frac{1}{2}} + [1 + \sin^2 \theta \cos^2 \psi]_{\frac{1}{2}; \frac{1}{2}} \\ &\quad [\cos^2 \theta - \sin^2 \theta e^{2i\phi}]_{\frac{1}{2}; \frac{1}{2}} [\cos^2 \theta - \sin^2 \theta e^{2i\psi}]_{\frac{1}{2}; \frac{1}{2}}; \end{aligned} \quad (7)$$

where to be consistent with the conventions for the transition amplitudes defined by Eq. (1), we have labeled the density matrix elements by the helicities of the particles. Since the helicity direction is defined as the momentum of the  $K$  in the final state, the only change is  $s \rightarrow s^0$  and  $s^0 \rightarrow 0$ .

The density matrix elements for the  $^+$  can be related to the photon density matrix elements in the  $^+$  production:

$$\rho_{s; s^0} = \frac{1}{N} \sum_{N; \gamma; \gamma^0} T_{s; N}^{\dagger} \rho_{\gamma; \gamma^0} (T_{0; 0; N}) \quad (8)$$

where  $N = \frac{1}{2} P_{\gamma; \gamma^0} T_{s; N}^{\dagger} T_{0; 0; N}$  is the normalization factor, and it has conventionally a factor 1/2 difference from the initial spin average and final spin summation [47]. Note that  $\rho_{\gamma; \gamma^0} = \frac{1}{2} (1 + P \cos 2\theta; \sin 2\theta; 0)$  is determined by the polarization direction  $P$  and the eigenvalue of the photon polarization states. As discussed in Ref. [47], for circularly polarized photons,  $P = P(0; 0; 1)$ , while for linearly polarized photons,  $P = P(\cos 2\theta; \sin 2\theta; 0)$ , where  $\theta$  is the angle between the photon polarization vector and the  $^+$  production plane ( $x$ - $z$  plane) [47], and  $P$  denotes the photon polarization degree in experiment. Given the eigenvalues for different polarization components of the photons, the corresponding density matrix elements for the  $^+$  can be defined:

$$\rho_{s; s^0} = \frac{1}{2N} \sum_N T_{s; N}^{\dagger} T_{0; 0; N} \quad (9)$$

$$T_{\frac{1}{2}; \frac{1}{2}}^0 = \frac{1}{2N} \sum_N T_{\frac{1}{2}; \frac{1}{2}}^N; \quad T_{\frac{1}{2}; \frac{1}{2}}^0 = \frac{1}{2N} \sum_N T_{\frac{1}{2}; \frac{1}{2}}^N; \quad (10)$$

$$T_{\frac{1}{2}; \frac{1}{2}}^1 = \frac{i}{2N} \sum_N T_{\frac{1}{2}; \frac{1}{2}}^N; \quad T_{\frac{1}{2}; \frac{1}{2}}^1 = \frac{i}{2N} \sum_N T_{\frac{1}{2}; \frac{1}{2}}^N; \quad (11)$$

$$T_{\frac{1}{2}; \frac{1}{2}}^2 = \frac{1}{2N} \sum_N T_{\frac{1}{2}; \frac{1}{2}}^N; \quad T_{\frac{1}{2}; \frac{1}{2}}^2 = \frac{1}{2N} \sum_N T_{\frac{1}{2}; \frac{1}{2}}^N; \quad (12)$$

Together with the specified polarization direction  $P$ , the  $^{+}$  decay distribution for the linearly polarized photon beams can be expressed as

$$W(\theta; \phi) = W^0(\cos \theta; \phi; 0) + P \cos 2\theta W^1(\cos \theta; \phi; 1) + P \sin 2\theta W^2(\cos \theta; \phi; 2); \quad (13)$$

where  $W$  ( $= 0, 1, 2, 3$ ) corresponds to the decay distributions with different photon polarizations. Easily, it can be seen that  $W^0$  is for the distribution with unpolarized photon,  $W^{1,2}$  with linearly polarized photon, and  $W^3$  with circularly polarized photon. The explicit expressions for  $W$  is given by Eq. (7), and can be simplified by taking into account parity conservation:

$$T_{\frac{1}{2}; \frac{1}{2}}^N = (-1)^N T_{\frac{1}{2}; \frac{1}{2}}^N; \quad (14)$$

which leads to

$$T_{\frac{1}{2}; \frac{1}{2}}^0 = T_{\frac{1}{2}; \frac{1}{2}}^0; \quad T_{\frac{1}{2}; \frac{1}{2}}^1 = -T_{\frac{1}{2}; \frac{1}{2}}^1; \quad (15)$$

for  $= 0, 1$ ; and

$$T_{\frac{1}{2}; \frac{1}{2}}^2 = T_{\frac{1}{2}; \frac{1}{2}}^2; \quad T_{\frac{1}{2}; \frac{1}{2}}^3 = -T_{\frac{1}{2}; \frac{1}{2}}^3; \quad (16)$$

for  $= 2, 3$ . On the other hand, the density matrix elements must be Hermitian:

$$T_{\frac{1}{2}; \frac{1}{2}}^0 = T_{\frac{1}{2}; \frac{1}{2}}^0; \quad (17)$$

which leads to:

$$\text{Re } T_{\frac{1}{2}; \frac{1}{2}}^0 = \text{Re } T_{\frac{1}{2}; \frac{1}{2}}^0; \quad \text{Im } T_{\frac{1}{2}; \frac{1}{2}}^0 = \text{Im } T_{\frac{1}{2}; \frac{1}{2}}^0; \quad \text{for } = 0, 1 \quad (18)$$

and

$$\text{Im } T_{\frac{1}{2}; \frac{1}{2}}^2 = \text{Im } T_{\frac{1}{2}; \frac{1}{2}}^2; \quad \text{Re } T_{\frac{1}{2}; \frac{1}{2}}^2 = \text{Re } T_{\frac{1}{2}; \frac{1}{2}}^2; \quad \text{for } = 2, 3; \quad (19)$$

Also note that elements with  $= 0$  are always real. Thus, the angular distribution for  $^{+}$  decay with different polarizations will be:

$$\begin{aligned} W^0(\cos \theta; \phi; 0) &= 2 T_{\frac{1}{2}; \frac{1}{2}}^0 + 2 \sin^2 \theta \text{Im } T_{\frac{1}{2}; \frac{1}{2}}^0; \\ W^1(\cos \theta; \phi; 1) &= 2 T_{\frac{1}{2}; \frac{1}{2}}^1 + 2 \sin^2 \theta \text{Im } T_{\frac{1}{2}; \frac{1}{2}}^1; \\ W^2(\cos \theta; \phi; 2) &= 2 \sin 2\theta \cos 2\phi T_{\frac{1}{2}; \frac{1}{2}}^2 - 2 [\cos^2 \theta + \sin^2 \theta \cos 2\phi] \text{Re } T_{\frac{1}{2}; \frac{1}{2}}^2; \\ W^3(\cos \theta; \phi; 3) &= 2 [\cos^2 \theta + \sin^2 \theta \cos 2\phi] \text{Re } T_{\frac{1}{2}; \frac{1}{2}}^3; \end{aligned} \quad (20)$$

where  $W^3$  does not contribute to the linearly polarized photon reaction. In the above equation, we have used the relation  $T_{\frac{1}{2}; \frac{1}{2}}^3 = T_{\frac{1}{2}; \frac{1}{2}}^3 = 0$ .

B.  $^{+}$  of  $1=2$

Assuming that the  $^{+}$  has a spin-parity  $1=2$ , the decay transition will not involve spin operators, and can be simply expressed as:

$$\hat{R}_{S_f; S} m; s_f; P = p^0 f^{(s; 1=2)} j^{+}; s; P = 0; i = C_{S_f; S}; \quad (21)$$

Following the above procedure, we have the angular distribution of  $\pi^+$  decay:

$$\begin{aligned} W^0(\cos\theta; \phi; \lambda) &= 2 \frac{1}{2} \frac{1}{2} ; \\ W^1(\cos\theta; \phi; \lambda) &= 2 \frac{1}{2} \frac{1}{2} ; \\ W^2(\cos\theta; \phi; \lambda) &= 2 \text{Re} \frac{2}{2} ; \frac{1}{2} ; \\ W^3(\cos\theta; \phi; \lambda) &= 2 \text{Re} \frac{3}{2} ; \frac{1}{2} ; \end{aligned} \quad (22)$$

where the isotropic distribution of the  $\pi^+$  decay is due to the relative S-wave between the  $K^+$  and  $n$ .

$$C. \quad \pi^+ \text{ of } 3=2^+$$

For  $\pi^+$  of spin-parity  $3=2^+$ , its decay transition operator is given by the Rarita-Schwinger field transition to a spinor and a vector field:

$$\begin{aligned} \hat{R}_{s_f; s} &= \langle n; s_f; P | p^0 \mathcal{P} | p; s; P \rangle = 0i \\ &= C^X \langle n | \frac{1}{2} s_f \frac{3}{2} s_i | e | p \rangle \\ &= C^0 \langle n | \frac{1}{2} s_f \frac{3}{2} s_i | D^1_0(\theta; \phi) \rangle; \end{aligned} \quad (23)$$

where  $e$  is the spherical vector presentation of an orthogonal set of cartesian unit vectors  $\hat{x}$ ,  $\hat{y}$ , and  $\hat{z}$ :

$$e_1 = \frac{1}{\sqrt{2}}(\hat{x} - i\hat{y}); \quad e_0 = \hat{z}; \quad (24)$$

Following the same strategy as the above, the  $\pi^+$  decay distribution can be obtained:

$$\begin{aligned} W(\cos\theta; \phi; \lambda) &= \frac{1}{3} + \cos^2\theta \frac{1}{2} \frac{1}{2} + \sin^2\theta \frac{3}{2} \frac{3}{2} - \frac{1}{3} \sin^2\theta \sin 2\phi \text{Im} \frac{1}{2} ; \frac{1}{2} - \sin^2\theta \sin 2\phi \text{Im} \frac{3}{2} ; \frac{3}{2} \\ &+ \frac{2}{3} \sin 2\phi \cos\theta \text{Re} \frac{1}{2} ; \frac{3}{2} - \frac{2}{3} \sin^2\theta \cos 2\phi \text{Re} \frac{1}{2} ; \frac{3}{2} - \frac{2}{3} \sin 2\phi \sin\theta \text{Im} \frac{1}{2} ; \frac{3}{2} \end{aligned} \quad (25)$$

for  $\lambda = 0, 1$ , and

$$\begin{aligned} W(\cos\theta; \phi; \lambda) &= \frac{1}{3} \sin 2\phi \cos\theta \frac{1}{2} ; \frac{1}{2} + \frac{4}{3} \cos^2\theta - \frac{1}{3} \sin^2\theta \cos 2\phi \text{Re} \frac{1}{2} ; \frac{1}{2} - \sin^2\theta \cos 2\phi \text{Re} \frac{3}{2} ; \frac{3}{2} \\ &+ \frac{2}{3} \sin^2\theta \text{Re} \frac{1}{2} ; \frac{3}{2} - \frac{2}{3} \sin 2\phi \sin\theta \text{Im} \frac{1}{2} ; \frac{3}{2} \\ &- \frac{2}{3} \sin 2\phi \cos\theta \text{Re} \frac{1}{2} ; \frac{3}{2} - \frac{2}{3} \sin^2\theta \sin 2\phi \text{Im} \frac{1}{2} ; \frac{3}{2} \end{aligned} \quad (26)$$

for  $\lambda = 2, 3$ , and with  $\frac{3}{2} \frac{1}{2} = 0$ . In the above two equations, parity conservation relation and the requirement of to be Hermitian have been used, and the elements are presented in the helicity frame. We note that for elements  $\frac{1}{2} ; \frac{1}{2}$  with  $j \neq j^0$ , their real (imaginary) parts are not independent of each other due to parity conservation and Hermitian. Also, it is found that  $\text{Im} \frac{0;1}{\frac{1}{2}; \frac{3}{2}} = \text{Im} \frac{0;1}{\frac{1}{2}; \frac{1}{2}}$  is not necessarily zero. However, this term is canceled out, which could suggest that there is no experimental access to this quantity by using the polarized photon beams.

### III. POLARIZATION OBSERVABLES

The advantage of polarization measurement is that the interference between different transition amplitudes can be highlighted by the asymmetries. Therefore, additional information on the transition dynamics can be gained. In theory, the study of the polarized beam asymmetries is also useful to partially avoid uncertainties arising from

the form factors, while the availability of experimental data will provide constraints on parameters introduced in a phenomenology.

With the polarized photon beams the polarized beam asymmetries can be measured via Eqs. (20), (22), (25) and (26). In particular, with the linearly polarized photons,  $W^{0;1;2}$  can be measured.

In principle, one can choose the polarization direction of the photons to derive as much information as possible. Equation 13 is general for linearly polarized photons. We thus can choose  $\theta = 90^\circ$  to polarize the photons along the y-axis, and  $\phi = 0$  to polarize the photons along the x-axis. By integrating over  $\theta$  and  $\phi$ , namely, summing over all the experimental events, we have respectively:

$$\begin{aligned} W_{\gamma}(\theta = 90^\circ; \phi) &= \int_{-1}^1 \int_0^{2\pi} dW^0(\cos\theta; \phi; 0) P \int_{-1}^1 \int_0^{2\pi} dW^1(\cos\theta; \phi; 1) \\ &= W^0(0) + P W^1(1); \end{aligned} \quad (27)$$

and

$$W_k(\theta = 0; \phi) = W^0(0) - P W^1(1); \quad (28)$$

which are cross sections for the two polarizations. In experiment, the polarized beam asymmetry can be defined as

$$A = \frac{W_{\gamma}(\theta = 90^\circ; \phi) - W_k(\theta = 0; \phi)}{W_{\gamma}(\theta = 90^\circ; \phi) + W_k(\theta = 0; \phi)} = \frac{W^1(1)}{W^0(0)}; \quad (29)$$

where  $(W_{\gamma} + W_k)$  corresponds to the unpolarized cross section.

For the circumstance where  $\pi^+$  has spin-parity  $\frac{1}{2}^-$  and  $\frac{1}{2}^+$ , the expression for the polarized beam asymmetry is the same:

$$A = \frac{\frac{1}{2}, \frac{1}{2}}{0, \frac{1}{2}} : \quad (30)$$

However, this does not suggest that these two configurations will have the same asymmetries. The values for the elements will be determined by underlying dynamics. Also note that our convention of polarized beam asymmetry has a sign difference as that of Ref. [48]. It can be seen by the decomposition of  $\frac{1}{2}, \frac{1}{2}$  in terms of the transition amplitudes  $T$ :  $\frac{1}{2}, \frac{1}{2} = \frac{1}{N} \text{Re}f T_{\frac{1}{2}, 1} T_{\frac{1}{2}, 1} + T_{\frac{1}{2}, 1} T_{\frac{1}{2}, 1} = g = W^0_{\frac{1}{2}, \frac{1}{2}}$ . The expression is essentially the same as that derived for pseudoscalar meson photoproduction on the nucleon. This is understandable since the spins of all the particles are the same as, e.g.,  $n \rightarrow p$ . Equation 30 also implies a direct access to element  $\frac{1}{2}, \frac{1}{2}$ , which is normalized by the differential cross section.

For  $3=2^+$ , the polarized beam asymmetry is

$$A\left(\frac{3}{2}\right) = \frac{\frac{1}{2}, \frac{1}{2} + \frac{1}{2}, \frac{3}{2}}{0, \frac{1}{2} + \frac{3}{2}, \frac{3}{2}}; \quad (31)$$

where  $2\left(\frac{0}{2}, \frac{1}{2} + \frac{0}{2}, \frac{3}{2}\right) = 1$  is the normalized cross section.

For  $3=2^+$ , explicit angular dependence is introduced into the  $\pi^+$  decay distribution by the photon polarization transfer, which makes it much more easier to clarify the configuration in experiment. In particular, for the case that  $\frac{0}{2}, \frac{3}{2}$  is much smaller than  $\frac{0}{2}, \frac{1}{2}$ , a clear signal can be seen by the  $\cos^2$  distribution with the  $\theta$ -angle distribution integrated out at  $\phi_{cm} = 0$ :

$$W(\theta) = 2 \left( \frac{1}{3} \frac{0}{2}, \frac{1}{2} + \frac{0}{2}, \frac{3}{2} \right) + \cos^2 \left( \frac{0}{2}, \frac{1}{2} - \frac{0}{2}, \frac{3}{2} \right); \quad (32)$$

If  $\frac{0}{2}, \frac{1}{2}$  and  $\frac{0}{2}, \frac{3}{2}$  are comparable, ambiguities will arise, and dynamic aspects have to be taken into account along with the analyses based on kinematics.

Elements  $\frac{2}{2}$  can be also measured by polarizing the photon along  $\theta = 45^\circ$ . For these three configurations, the polarization asymmetry can be defined as

$$B\left(\frac{1}{2}\right) = \frac{\text{Re} \frac{2}{2}, \frac{1}{2}}{0, \frac{1}{2}}; \quad (33)$$

$$B\left(\frac{1}{2}\right) = \frac{\text{Re} \frac{2}{\frac{1}{2}; \frac{1}{2}}}{3 \frac{0}{\frac{1}{2}; \frac{1}{2}}}; \quad (34)$$

and

$$B\left(\frac{3}{2}\right) = \frac{2\text{Re} \frac{2}{\frac{1}{2}; \frac{1}{2}} + 2^P \text{Re} \frac{2}{\frac{1}{2}; \frac{3}{2}}}{3 \left( \frac{0}{\frac{1}{2}; \frac{1}{2}} + \frac{0}{\frac{1}{2}; \frac{3}{2}} \right)} \quad (35)$$

where different elements can be detected.

For  $^{+}$  of  $3=2^{+}$ , it is likely that experimental analyses of its decay distributions has been informative of its properties. Therefore, as follows, we will concentrate on the production of the  $1=2^{+}$  and  $1=2^{-}$  configurations for which the transfer of the beam polarized to the  $^{+}$  can only be distinguished through their different dynamical properties. Also, we will adopt the convention of Ref. [48] to include the additional sign for the polarized beam asymmetry.

#### A. Polarized beam asymmetry for $^{+}$ of $1=2^{+}$ in the Born limit

For the  $^{+}$  of  $1=2^{+}$ , the effective Lagrangian introduces four transition amplitudes in the Born approximation limit as shown by Fig. 1. The leading terms are similar to the case of  $n!$   $p$ , which would be useful for the analyses. The transition amplitudes can be expressed as:

$$M_{fi} = M^c + M^t + M^s + M^u; \quad (36)$$

where the four transitions are given by

$$\begin{aligned} M^c &= ie_0 g_{NK} \quad {}_5A_{NK}; \\ M^t &= \frac{ie_0 g_{NK}}{t - M_K^2} \quad {}_5(q - k)(2q - k) A_{NK}; \\ M^s &= g_{NK} \quad {}_5\theta_K \frac{[(k + P) + M_n]}{s - M_n^2} e_n + \frac{i_n}{2M_n} k A_N; \\ M^u &= g_{NK} e + \frac{i}{2M} k A \frac{[(P - k) + M]}{u - M^2} \quad {}_5\theta_{KN}; \end{aligned} \quad (37)$$

where  $e_0$  is the positive unit charge. In the s-channel the vector coupling vanishes since  $e_n = 0$ . We define the coupling constant  $g_{NK} = g_A M_n = f$  with the axial vector coupling  $g_A = 5=3$ , while the decay constant is given by:

$$f = g_A \quad {}_1 \frac{p_0}{E_n + M_n} \frac{\mathbf{p}^{0,3} (E_n + M_n)}{4 M_n} \quad {}^{1=2}_{+! K+n}; \quad (38)$$

where  $p^0$  and  $p_0$  are momentum and energy of the kaon in the  $^{+}$  rest frame, and  $E_n$  is the energy of the neutron. For the range of  $^{+! K+n} = 5$  to 25 MeV,  $g_{NK} = 2.09$  to 4.68. We adopt  $g_{NK} = 2.96$  for  $^{+! K+n} = 10$  MeV in the calculations.

The  $^{+}$ 's magnetic moment  $\mu = (1 + )=2M$  is estimated in the model of Jaffe and Wilczek [12]:

$$\mu = \sum_{i=1}^3 \frac{e_i}{2m_i} (i + l_i); \quad (39)$$

where  $e_1$  ( $e_2$ ) and  $m_1$  ( $m_2$ ) denote the charge and mass of the (ud) clusters, and  $e_3$  and  $m_3$  of the  $s$ ;  $= 2s$  denotes the Pauli matrices. For (ud) (ud)s, the isospin wavefunction belongs to SU(3) symmetric representation 10, and u-d couples to spin zero clusters. Taking into account the parity of the s, the lowest energy state of  $1=2^{+}$  requires the total orbital angular momentum to be odd and at least  $L = i l_i = 1$ , where the bold number denotes the angular momentum vector. Since the (ud) clusters are identical, we choose the Jacobi coordinate to construct the spatial wavefunction. As a result [49], the magnetic moment can be rewritten as

$$= \frac{e_0}{6m_3} {}_3 + \frac{e_0}{6m_1} {}_1 + \frac{e_0}{6M} \left( \frac{m_3}{m_1} + \frac{2m_1}{m_3} \right) {}_1; \quad (40)$$

where  $l$  and  $l$  are the orbital angular momenta for the internal coordinates in the c.m. system, and  $L = l + l$ ;  $e_0$  is the unit charge. For the simplest case that either  $l$  or  $l$  to be excited one unit, by taking the z-projection  $m_z = 1$ , we have

$$= \frac{e_0}{2M} \left[ \frac{M}{9m_3} + \frac{2M}{9m_1} b^2 + \frac{1}{9} \left( \frac{m_3}{m_1} + \frac{2m_1}{m_3} \right) a^2 \right]; \quad (41)$$

where  $a^2$  and  $b^2$  denote the probability of exciting  $l$  and  $l$  by one unit, and  $a^2 + b^2 = 1$  as required by the normalization. Adopting quark and diquark masses of Ref. [12]:  $m_3 = 500$  MeV for  $s$  and  $m_1 = m_2 = 720$  MeV, we have  $a^2 = 0.094$  ( $e_0 = 2M$ ) with  $a^2 = b^2 = 1/2$ ,  $0.055$  ( $e_0 = 2M$ ) with  $a^2 = 1$  and  $b^2 = 0$ , and  $0.133$  ( $e_0 = 2M$ ) with  $a^2 = 0$  and  $b^2 = 1$ . This rough estimate suggests a small magnetic moment for the  $\Lambda^+$  in the Jaffe and Wilczek's picture. We will take the value  $a^2 = 0.13$  ( $e_0 = 2M$ ), i.e. the anomalous magnetic moment  $\mu = 0.87$ , in the calculation as follows.

To proceed, we make a nonrelativistic expansion of the above transition amplitudes, and adopt the typical nonrelativistic quark model wavefunctions for the form factor, which is essentially a Gaussian distribution for the wavefunction overlaps [50]. This treatment is examined in  $\Lambda^+ \rightarrow p$  at low energies. In Fig. 2, we present the calculation of cross sections with the above effective Lagrangian. In comparison with the full quark model calculation (dashed curve) [50], the form factor adopted account for the cross section reasonably well, and note that only the Delta resonance is included here. This test also shows that the contact term and t-channel exchange play important roles near threshold, which will be a guide in the  $\Lambda^+$  production.

In Fig. 3, the differential cross sections are presented for  $\Lambda^+ \rightarrow K^+ p$  at  $W = 2.1$  and  $2.5$  GeV, which exhibit forward peakings. The contact term accounts for the forward peaking and is examined by suppressing it from contributing as shown by the dashed curves. This feature is similar to the case of  $\Lambda^+ \rightarrow p \gamma$  photoproduction. We also examine the role played by the s- and u-channels by switching off their contributions (dotted curves). It shows that the dominant contributions are from the contact term and t-channel exchange. The bump structure arising from the dashed curves are due to the relatively strong t-channel kaon exchange. As we will see later, in contrast with the  $\Lambda^+$  of  $1=2$ , the important role played by the contact term will be a signature for the  $\Lambda^+$  of  $1=2^+$  in the polarized beam asymmetries in the Born limit.

Qualitatively, the photoproduction of  $\Lambda^+$  of  $1=2^+$  is similar to the pseudoscalar meson photoproduction and will have the typical spin structures of the well-known CGLN amplitudes [51]:  $\sigma_{\text{tot}}$ ,  $\sigma_{\text{pol}}$  ( $k$ ),  $\sigma_{\text{qq}}$ , and  $\sigma_{\text{qk}}$ . It makes the kinematics  $\theta_{\text{cm}} = 0$  and  $180^\circ$  special since only the term of  $\sigma_{\text{qq}}$  will contribute. This term will either raise or lower the initial neutron spin projection by one unit. Therefore, it will contribute to either  $T_{\frac{1}{2}, \frac{1}{2}}$  or  $T_{\frac{1}{2}, -\frac{1}{2}}$  for a fixed polarization  $\frac{1}{2}$ . As a result,  $T_{\frac{1}{2}, \frac{1}{2}}$  will vanish at  $\theta_{\text{cm}} = 0$  and  $180^\circ$ , and thus  $\sigma_{\text{qq}} = 0$  at these two scattering angles. More clear evidence for the importance of the contact term can be seen in the polarized beam asymmetry through its interferences with other terms. In Fig. 4,  $\sigma_{\text{pol}}$  is presented at two energies in parallel to Fig. 3.

The asymmetries arising from the Born terms (solid curves) are relatively small, which are also similar to the case of  $\Lambda^+ \rightarrow p \gamma$  photoproduction. By switching off the contact term, we obtain the dashed curves, which are strongly stretched towards  $\pm 1$ . This feature is accounted for by the dominant t-channel exchange (with the absence of the contact term) in comparison with the relatively small s- and u-channels: the exclusive t-channel will analytically lead to  $\sigma_{\text{pol}} = \pm 1$ . However, due to the interference of the contact transition, of which the exclusive contribution leads to vanishing asymmetries, the asymmetry exhibits a rather small deviations from zero. This feature is independent of the form factors since they will cancel out. In this sense, additional information about the  $\Lambda^+$  can be derived from polarized beam asymmetries. Nevertheless, the contact term in  $1=2^+$  production will provide a clear way to distinguish it from the  $1=2$  if the transitions are only via the Born terms.

## B. Polarized beam asymmetry for $\Lambda^+$ of $1=2$ in the Born limit

For  $\Lambda^+$  of  $1=2$ , the effective Lagrangian for the  $\Lambda^+ n K$  system (Eq. (2)) conserves parity and is gauge invariant. This suggests that the electromagnetic interaction will not contribute to the contact term, which can be also seen in the leading term of nonrelativistic expansion, where the derivative operator is absent. The Born approximation therefore includes three transitions (Fig. 1(b), (c) and (d)): t-channel kaon exchange, s-channel nucleon exchange, and u-channels  $\Lambda^+$  exchange. The invariant amplitude can be written as

$$M_{fi} = M^t + M^s + M^u; \quad (42)$$

where the three transitions are given by

$$M^t = \frac{e_0 g_{\Lambda N K}}{t - M_K^2} (2q - k) \cdot A_N;$$

$$\begin{aligned}
M^s &= g_{NK} K \frac{[(k + \frac{1}{2}) + M_n]}{s M_n^2} e_n + \frac{i_n}{2M_n} k A N; \\
M^u &= g_{NK} e + \frac{i}{2M} k A \frac{[(\frac{1}{2} - k) + M]}{u M^2} N K;
\end{aligned} \tag{43}$$

where the coupling constant  $g_{NK} = [4 M_{\pi}^2 + \frac{1}{2} K^+ n = \frac{1}{2} j(E_n + M_n)]^{1/2}$  has a range of 0.43–0.96 with  $\frac{1}{2} K^+ n = 5$  to 25 MeV, and turns out to be much smaller than  $1=2^+$  coupling. We adopt  $g_{NK} = 0.61$  corresponding to  $\frac{1}{2} K^+ n = 10$  MeV in the calculation.

If  $\frac{1}{2}^+$  has spin-parity  $1=2^-$ , one may simply estimate its magnetic moment as the sum of (us) and (udd) clusters, of which the relative orbital angular momentum is zero. Assuming these two clusters are both color singlet, the total magnetic moment of this system can be written as

$$= \frac{2e_0}{6m_u} + \frac{e_0}{6m_s} - \frac{e_0}{3m_u} = \frac{e_0}{6m_s}; \tag{44}$$

which leads to a small anomalous magnetic moment taking into account  $3m_s \gg M$ . However, since such a simple picture may not be sufficient, we also include  $\mu_p = 1.79$  to make a sensitivity test.

In Fig. 5, the differential cross sections for  $1=2^-$  production are presented at  $W = 2.1$  and 2.5 GeV. The solid curves are results of the Born terms, while the dotted curves denote calculations for the exclusive t-channel, i.e. with the s- and u-channel Born terms eliminated. Near threshold, the s- and u-channels turn out to be important as shown by the dotted curve, and explains the rather flat distribution. Above threshold, the t-channel kaon exchange becomes more and more important and produces a bump structure in the forward angle region. The strong forward peaking appearing in  $1=2^+$  is absent here. The cross sections for  $\mu_p = 1.79$  (dashed and dot-dashed) are also presented. In comparison with the solid curves, quite significant sensitivity to  $\mu_p$  appears near threshold.

The t-channel dominance above the threshold region leads to specific signature of the  $1=2^-$  in the polarization asymmetries. Qualitatively, given an exclusive contribution from the t-channel kaon exchange, the transition amplitude will have a structure of  $q$ , which is spin-independent. In this circumstance, the polarized beam asymmetry becomes  $A = -1$  (or  $w = +1$ ) due to the exact cancellation of the angular parts in  $\frac{0}{2} i_{\frac{1}{2}}$  and  $\frac{1}{2} i_{\frac{1}{2}}$ . In Fig. 6, the asymmetry  $w$  produced by the Born terms is shown by the solid curves at  $W = 2.1$  and 2.5 GeV. The dotted lines denote the constant asymmetry  $+1$  produced by the exclusive t-channel kaon exchange. The inclusion of the s- and u-channels violates the constant  $+1$  asymmetry, and results in the vanishing asymmetries at  $\phi_{cm} = 0$  and  $180^\circ$ . In particular, due to the dominance of the s- and u-channels near threshold, the asymmetry appears to be small. With the increasing energies the t-channel becomes more and more important, and will stretch the asymmetries ( $w$ ) towards  $+1$  with large values. This is characteristic for  $1=2^-$ , and makes it different from the moderate behavior of  $1=2^+$ , e.g., at  $W = 2.5$  GeV. We also present the results for  $\mu_p = 1.79$  (dashed and dot-dashed). Quite sizeable effects appear at middle angles, while the vanishing asymmetries at forward and backward angles are not sensitive to the  $\frac{1}{2}^+$ 's anomalous magnetic moment.

Certain points can be learned here:

- i) For the Born terms, the  $\frac{1}{2}^+$  of different parities results in an order of magnitude difference in the cross sections. This is consistent with other model calculations [43, 44, 45]. However, it also shows that the cross section is very sensitive to the empirical form factors adopted, which may lead to large uncertainties in the model predictions.
- ii) The polarized beam asymmetry has less dependence on the form factor than the cross section. For the Born terms, as shown by Figs. 4 and 6, the asymmetries at  $W = 2.5$  GeV exhibit completely different behaviors for the  $\frac{1}{2}^+$  of  $1=2^+$  and  $1=2^-$ , which should make these two configurations distinguishable.
- iii) For exclusive contributions, e.g. the contact term plus t-channel in the production of  $1=2^+$ , and the t-channel of  $1=2^-$ , we also find significantly different features arising from the polarized beam asymmetries.

Summarily, supposing the  $\frac{1}{2}^+$  is produced dominantly via Born terms, the polarized beam asymmetry measurement incorporating with the cross section will be able to determine its quantum numbers. However, in reality such an assumption is too drastic since other mechanisms may interfere and even play dominant roles with increasing energies. To proceed and investigate the effects from other mechanisms, we will include the vector meson  $K$  exchange in the model and study its impact on the cross sections and polarized beam asymmetries.

### C. $K$ exchange in $\frac{1}{2}^+$ of $1=2^+$ production

The role played by vector meson exchanges in pseudoscalar meson photoproduction is still a controversial issue in theoretical phenomenology. According to the duality argument [52], the inclusion of vector meson exchange in association with a complete set of s-channel resonances may result in double-counting of the cross sections. Therefore,

one in principle, can include either all s-channel states or a complete set of t-channel trajectories in a full calculation. In reality, difficulty arises from the lack of knowledge about these two extremes, and empirical phenomenologies will generally include the leading contributions of both channels taking into account partially their different roles at different kinematical regions.

The exotic  $\pi^+$  production would complicate such an issue if any s- and t-channel processes beyond the Born approximation are important. Certainly, this relevance deserves a full independent study. In this work, we will only empirically include the  $K$  meson exchange in  $\pi^+ K^-$ . The essential concern here is its effects on the polarized beam asymmetries: will it change the basic features produced by the Born terms near threshold?

The effective Lagrangian for  $K^- K^0$  is given by

$$\mathcal{L}_{K^- K^0} = \frac{ie_0 g_{K^- K^0}}{M_K} (\partial_\mu A^\mu \partial_\nu V^\nu K^- + \text{H.c.}); \quad (45)$$

where  $V^\mu$  denotes the  $K^-$  field;  $g_{K^- K^0} = 0.744$  is determined by the  $K^-$  decay width  $\Gamma_{K^- \rightarrow \pi^0 \ell^- \bar{\nu}_\ell} = 50 \text{ keV}$  [53].

The  $K^- N$  interaction is given by

$$\mathcal{L}_{K^- N} = g_{N K^-} \left( \vec{\sigma} \cdot \vec{\partial} + \frac{1}{2M} \partial_\mu \partial^\mu \right) V^\mu N + \text{H.c.}; \quad (46)$$

where  $g_{N K^-}$  and  $\vec{\sigma}$  denote the vector and tensor couplings, respectively. So far, there is no experimental information about these two couplings. A reasonable assumption based on an analogue to vector meson exchange in pseudoscalar meson production is that  $\vec{g}_{N K^-} = \vec{g}_{N K^0}$ . For the tensor coupling, we assume  $\sigma_j = \sigma_j = 3/71$ , the same as  $NN$  tensor coupling but with an arbitrary phase. Therefore, four sets of different phases are possible.

In Fig. 7, the differential cross sections for  $l=2^+$  production at  $W = 2.1$  and  $2.5 \text{ GeV}$  are presented. The four possible phases:  $(g_{N K^-}; \sigma) = (2/8; 3/71)$  and  $(+2/8; +3/71)$  corresponding to the dashed and dotted curves in the upper two figures, and  $(-2/8; +3/71)$  and  $(+2/8; -3/71)$  to the dashed and dotted curves in the lower two figures, are shown in contrast with the calculations without the  $K^-$  exchange (solid curves). It shows that the  $K^-$  exchange with its coupling comparable with  $g_{N K^-}$  will play an important role. The change of the parameter phases results in significant changes to the cross sections. In particular, the tensor coupling turns out to be dominant. The interference of the  $K^-$  exchange in the polarized beam asymmetry also becomes important. In Fig. 8, the polarized beam asymmetry is presented in parallel to Fig. 7. It shows that near threshold the effects from the  $K^-$  exchange is quite small. In contrast with its effects in the differential cross section near threshold, the small change to the asymmetries can be understood by the overall enhancement or cancellation within the amplitudes throughout the scattering angles as shown by the curves for  $W = 2.1 \text{ GeV}$  in Fig. 7. At  $W = 2.5 \text{ GeV}$  quite significant asymmetries are produced by the phase changes.

#### D. $K^-$ exchange in $\pi^+$ of $l=2^-$ production

We also include the  $K^-$  exchange in the  $l=2^-$  production, in which the  $K^- N$  interaction is given by

$$\mathcal{L}_{K^- N} = g_{N K^-} \left( \vec{\sigma} \cdot \vec{\partial} + \frac{1}{2M} \partial_\mu \partial^\mu \right) V^\mu N + \text{H.c.}; \quad (47)$$

Similar to the case of  $l=2^+$ , we assume  $\vec{g}_{N K^-} = \vec{g}_{N K^0}$ . In the calculation we choose the anomalous magnetic moment  $\sigma_j = 0.371$ , which is ten times smaller than that in the production of  $l=2^+$ . This choice is based on that  $g_{N K^-} = 0.61$  is also about one magnitude smaller than that in the production of  $l=2^+$ . In Fig. 9, the cross section for  $l=2^-$  production at  $W = 2.1$  and  $2.5 \text{ GeV}$  are presented. The four possible phases:  $(g_{N K^-}; \sigma) = (0.61; 0.371)$  and  $(+0.61; +0.371)$  corresponding to the dashed and dotted curves in the upper two figures, and  $(-0.61; +0.371)$  and  $(+0.61; -0.371)$  to the dashed and dotted curves in the lower two figures, are shown in contrast with the calculations without the  $K^-$  exchange (solid curves). It shows that the forward cross section is dominated by the  $K^-$  exchange. Near threshold, the cancellation between the Born terms and  $K^-$  exchange of two phases can even lead to vanishing cross sections, while the other two phases lead to forward peaking. Above the threshold region, the Born terms become relatively small and forward peaking due to the  $K^-$  exchange appears in those four sets of phases.

A rather interesting feature arising from the  $K^-$  exchange in the production of  $l=2^-$  is that the cross sections increase drastically. For one of the phases,  $(g_{N K^-}; \sigma) = (+0.61; +0.371)$  at  $W = 2.5 \text{ GeV}$  (dotted curve in the upper-right figure of Fig. 9), the cross sections at forward angles are comparable with the  $l=2^+$  production with  $(g_{N K^-}; \sigma) = (+2/8; 3/71)$  (dotted curve in the lower-right figure of Fig. 7). As mentioned at the beginning that so far little information about the form factors has been available. Therefore, large uncertainties could be with the

model predictions for the cross sections. In this sense, a single measurement of the cross sections may not be able to distinguish these two parities if the  $K$  exchange has large contributions.

More information about the  $^{+}$  properties can be obtained from the polarization asymmetries. In Fig. 10, we present the calculations for  $w$  in parallel to the cross sections. Significant sensitivities to the  $K$  exchange are found, and interesting feature arises from its interferences. For  $(g_{NK}; \delta) = (0.61; 0.371)$  (dashed curves in the upper and lower figures), significantly large positive asymmetries appear near threshold. This is a unique feature since large positive asymmetries cannot be produced in all other phase sets and in the production of  $1=2^{+}$ . However, as shown by the dotted curves, asymmetries produced by phase sets  $(+0.61; -0.371)$  are generally small. These could mix up with the production of  $1=2^{+}$  near threshold if the measurement is only carried out in that energy region. Fortunately, taking into account the energy evolution of the asymmetries and cross sections, these two parities are still distinguishable from each other.

#### IV. DISCUSSIONS AND SUMMARIES

We investigated the possibility of using polarized photon beams to distinguish the quantum numbers of  $^{+}$  in experiment. The polarization of the photon beams transfers information of the  $^{+}$  configurations through the interference among the transition amplitudes, from which insights into the dynamical role played by the  $^{+}$  can be gained. We first examined the kinematics by comparing the angular distributions of  $^{+}$  decays with different quantum numbers. It showed that a clear  $\cos^2$  distribution after the sum over all the forward production events of all  $\theta$ -angles would be evidence for  $3=2^{+}$  configuration. For  $^{+}$  of  $1=2^{+}$  and  $1=2^{-}$ , the difference arising from the angular distributions of  $^{+}$  decay is strongly related to the dynamics of the production mechanism. In the Born approximation limit, the decay distributions for these two configurations will both become isotropic. Because of this, a coherent investigation of the production dynamics and the kinematical analysis is necessary.

So far, the theoretical calculation of the cross sections has been strongly model-dependent though it suggests significant difference between  $1=2^{+}$  and  $1=2^{-}$ . For instance, the coupling strength  $g_{NK}$  is determined by the  $^{+}$  decay width, which however has still large uncertainties. Also, the form factors as well as the roles played by other mechanisms, e.g.,  $K$  exchange and spin  $3/2$  state, are almost unknown. Due to such complexities, the measurement of cross sections could be a premier reference for distinguishing these two configurations, but hardly the only one. Other observables are also needed not only to pin down the  $^{+}$ 's quantum numbers, but also constrain theoretical phenomenologies.

Based on the investigations of this work, the following points concerning the  $^{+}$ 's quantum numbers and the photoproduction mechanisms can be learned:

- i) It seems very likely that a flat distribution near threshold will unambiguously refer to  $1=2^{-}$  for  $^{+}$ . For other situations, measurements of multi-observables are needed.
- ii) With the same total width for the  $^{+}$ , and assuming the same form factors, the cross section for  $1=2^{+}$  is much larger than  $1=2^{-}$  in the Born limit. This is consistent with other model calculations [43, 44, 45].
- iii) The exclusive Born terms of  $1=2^{+}$  production generally produce small negative values of asymmetries, while those of  $1=2^{-}$  produce rather large positive asymmetries above the threshold region. This feature is useful if the Born terms are the dominant contributions in the  $^{+}$  production.
- iv) The polarized beam asymmetry turns out to be sensitive to the  $K$  exchange, which eventually requires a better understanding of the  $NK$  coupling. In the case of weak  $NK$  coupling, the measurement of polarized beam asymmetries above the threshold region will be decisive on the  $^{+}$ 's quantum numbers as summarized in iii). For a strong  $NK$  coupling as  $NK$ , although the situation will be complicated, the asymmetry measurement in association with the cross section can still provide more information about the  $^{+}$ .
- v) Contributions from other spin states in the  $s$ - and  $u$ -channels may also become important. As shown by the dotted curves in Fig. 3, the  $s$ - and  $u$ -channel Born terms have sizeable contributions even above the reaction threshold. Other states, e.g., spin  $3/2$  one, may produce non-negligible effects at certain kinematics.

In brief, incorporating with the cross section observable, it seems likely that the polarized beam asymmetry will be able to provide additional information about the  $^{+}$  properties, which should be useful for determining its quantum numbers. The full angle detectors at SP Ring-8, JLab, ELSA, and ESRF will have a great advantage for such an exploration.

#### Acknowledgement

Special acknowledgement goes to F.E. Close for generously sharing many of his enlightening ideas and suggestions, and for many instructive comments on this work. The author thanks J.S. Al-Khalili for many useful discussions during

preparing this paper. The author also thanks K. Hicks and W.-J. Schille for responses related to their experiments. Useful communications with S.L. Zhu, and J. Kellie are acknowledged. This work is supported by grants from the U.K. Engineering and Physical Sciences Research Council (Grant No. GR/R78633/01).

- 
- [1] T. Nakano et al. [LEPS Collaboration], Phys. Rev. Lett. 91, 012002 (2003).
  - [2] V. Barin et al. [DIANA Collaboration], Phys. Atom. Nucl. 66, 1715 (2003) [Yad. Fiz. 66, 1763 (2003)]; hep-ex/0304040.
  - [3] S. Stepanyan et al. [CLAS Collaboration], hep-ex/0307018.
  - [4] J. Barth et al. [SAPHIR Collaboration], Phys. Lett. B 572, 127 (2003); hep-ex/0307083.
  - [5] K. Hicks, Talk given at Hadron2003, (2003).
  - [6] H. J. Lipkin, Phys. Lett. B 195, 484 (1987); C. Gignoux, B. Silvestre-Brac, and J. M. Richard, Phys. Lett. B 193, 323 (1987); S. Fleck, C. Gignoux, J. M. Richard, and B. Silvestre-Brac, Phys. Lett. B 220, 616 (1989); J. Leandri and B. Silvestre-Brac, Phys. Rev. D 40, 2340 (1989); S. Takeuchi, S. Nussinov, and K. Kubodera, Phys. Lett. B 318, 1 (1993); D. Oriska, N. N. Scoccola, Phys. Lett. B 299, 338 (1993); S. Zouzou and J. M. Richard, Few Body Syst. 16, 1 (1994); Y. Oh, B. Y. Park, D. P. Min Phys. Rev. D 50, 3350 (1994); C. K. Chow, Phys. Rev. D 53, 5108 (1996); M. Genovese, J. M. Richard, F. L. Stancu, and S. Pepin, Phys. Lett. B 425, 171 (1998);
  - [7] H. Gao and B. Q. Ma, Mod. Phys. Lett. A 14, 2313 (1999).
  - [8] T. H. R. Skyrme, Proc. Royal Soc. A 260, 127 (1961); Nucl. Phys. 31, 556 (1962).
  - [9] D. D. Iakonov, V. Petrov, and M. Polyakov, Z. Phys. A 359, 309 (1997).
  - [10] F. L. Stancu and D. Oriska, Phys. Lett. B 575, 242 (2003); hep-ph/0307010.
  - [11] F. E. Close and N. A. Tornqvist, J. Phys. G 28, R249 (2002).
  - [12] R. Jaffe and F. Wilczek, hep-ph/0307341.
  - [13] M. Karliner and H. J. Lipkin, hep-ph/0307343; hep-ph/0307243.
  - [14] S. Capstick, P. R. Page, and W. Roberts, Phys. Lett. B 570, 185 (2003); hep-ph/0307019.
  - [15] S. Nussinov, hep-ph/0307357.
  - [16] R. W. Gothe and S. Nussinov, hep-ph/0308230.
  - [17] R. A. Amdt, I. I. Strakovsky, and R. L. Workman, Phys. Rev. C 68, 042201 (2003); nucl-th/0308012.
  - [18] J. Haidenbauer and G. K Rein, Phys. Rev. C 68, 052201 (2003); hep-ph/0309243.
  - [19] C. E. Carlson, C. D. Carone, H. J. Kwee, and V. Nazaryan, Phys. Lett. B 573, 101 (2003); hep-ph/0307396.
  - [20] D. Borisyuk, M. Faber, and A. Kobushkin, hep-ph/0307370.
  - [21] M. Paszlowicz, Phys. Lett. B 575, 234 (2003); hep-ph/0308114.
  - [22] T. D. Cohen and R. F. Lebed, hep-ph/0309150.
  - [23] N. Itzhaki, I. R. Kabanov, P. Ouyang, and L. Rastelli, hep-ph/0309305.
  - [24] K. Cheung, hep-ph/0308176.
  - [25] L. Ya. Glozman, Phys. Lett. B 575, 18 (2003); hep-ph/0308232.
  - [26] B. K. Jennings and K. Maltman, hep-ph/0308286.
  - [27] F. Huang, Z. Y. Zhang, Y. W. Yu, and B. S. Zou, hep-ph/0310040.
  - [28] Y. Oh, H. Kim, and S. H. Lee, hep-ph/0310117.
  - [29] D. D. Iakonov and V. Petrov, hep-ph/0310212.
  - [30] R. Bijker, M. M. Giannini, and E. Santopinto, hep-ph/0310281.
  - [31] D. E. Kahana and S. H. Kahana, hep-ph/0310026.
  - [32] S. M. Gerasyuta and V. I. K ochkin, hep-ph/0310225; hep-ph/0310227.
  - [33] S. L. Zhu, Phys. Rev. Lett. 91, 232002 (2003); hep-ph/0307345.
  - [34] R. D. M.atheus et al., hep-ph/0309001.
  - [35] J. Sugiyama, T. Doi, and M. Oka, hep-ph/0309271.
  - [36] S. Sasaki, hep-lat/0310014.
  - [37] F. C. Siskor, Z. Fodor, S. D. Katz, and T. G. Kovacs, hep-lat/0309090.
  - [38] F. E. Close, Talk given at Hadron2003, (2003); private communications.
  - [39] Ya. I. Aizimov, R. A. Amdt, I. I. Strakovsky, and R. L. Workman, nucl-th/0307088.
  - [40] During the writing of this manuscript, evidence for another exotic state  $\chi_{3=2}$  with  $S = 2$  and  $Q = 2$  was reported by NA 49 collaboration. See C. A. J. et al., [NA 49 Collaboration], hep-ex/0310014.
  - [41] M. V. Polyakov and A. Rathke, hep-ph/0303138.
  - [42] T. Hyodo, A. Hosaka, and E. Oset, nucl-th/0307105.
  - [43] S. I. Nam, A. Hosaka, and H. Ch. Kim, hep-ph/0308313.
  - [44] W. Liu and C. M. Ko, Phys. Rev. C 68, 045203 (2003); nucl-th/0308034; nucl-ph/0309023.
  - [45] Y. Oh, H. Kim, and S. H. Lee, hep-ph/0310019.
  - [46] M. E. Rose, Elementary theory of angular momentum, (John Wiley, New York, 1957).
  - [47] K. Schilling, P. Seyboth, and G. Wolf, Nucl. Phys. B 15, 397 (1970).
  - [48] R. L. Walker, Phys. Rev. 182, 1729 (1969).
  - [49] Q. Zhao, work in progress.
  - [50] Q. Zhao, J. S. Alhalili, Z. P. Li, and R. L. Workman, Phys. Rev. C 65, 065204 (2002).

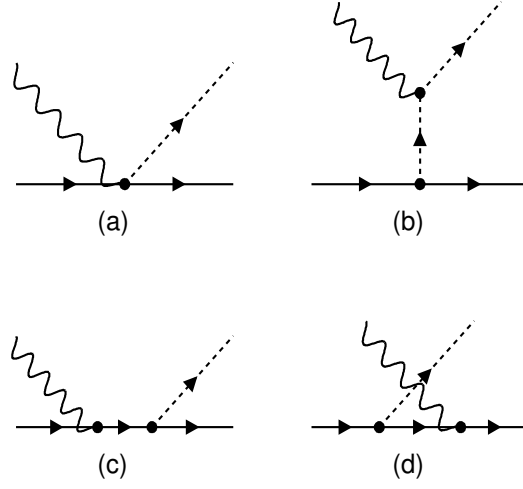


FIG. 1: Feynman diagrams for  $\pi^+$  photoproduction in the Born approximation.

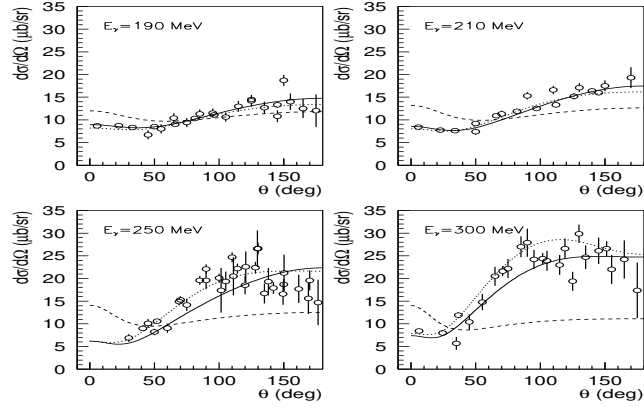


FIG. 2: Differential cross sections for  $\pi^+$  at  $E_\gamma = 190, 210, 250,$  and  $300$  MeV. The solid curves are results for Born term plus  $\Delta$ ; dashed curves for Born terms; dotted curves for the full quark model calculations [50].

[51] G.F. Chew, M.L. Goldberger, F.E. Low, and Y. Nambu, Phys. Rev. 106, 1345 (1957).

[52] R. Dolen, D. Horn, and C. Schmid, Phys. Rev. 166, 1768 (1966).

[53] D.E. Groom et al. (Particle Data Group), Eur. Phys. J. C 15, 1 (2000).

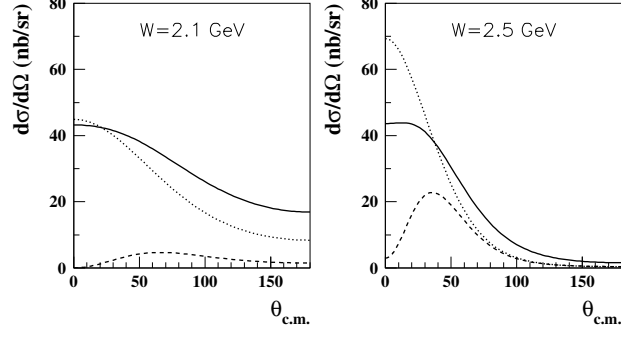


FIG. 3: Differential cross sections for  $n \rightarrow K^+$  with  $J^P$  of  $1=2^+$  at  $W = 2.1$  and  $2.5$  GeV in the Bom limit. The solid curves denote the results for the Bom terms; the dashed curves denote the results without the contact term; and the dotted curves denote the results without the s- and u-channel Bom contributions.

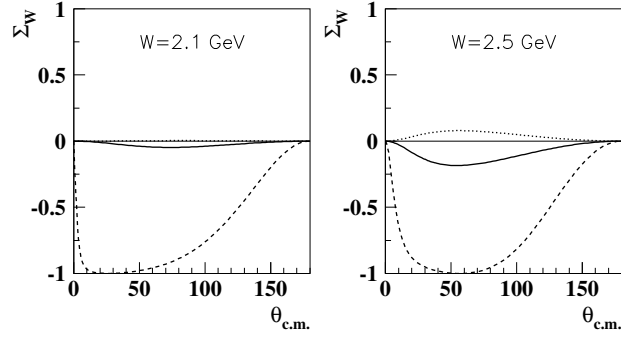


FIG. 4: Polarized beam asymmetries for  $n \rightarrow K^+$  with  $J^P$  of  $1=2^+$  at  $W = 2.1$  and  $2.5$  GeV in the Bom approximation limit. The notations are the same as Fig. 3.

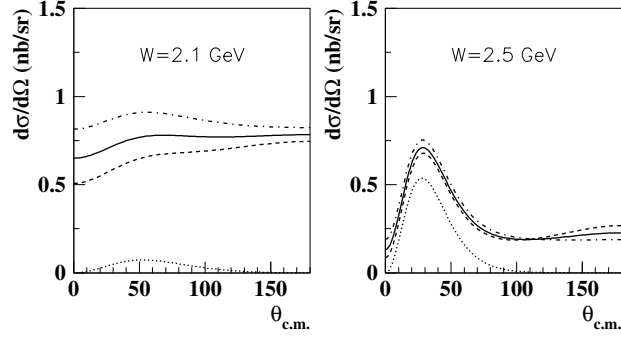


FIG. 5: Differential cross sections for  $n \rightarrow K^+ \pi^0$  with  $\pi^0$  of  $l=2$  at  $W = 2.1$  and  $2.5$  GeV in the Born limit. The solid curves denote the results for the Born terms; the dotted curves denote the results for the exclusive t-channel; the dashed and dot-dashed curves denote the results for  $\pi^0 = 1:7$ , respectively.

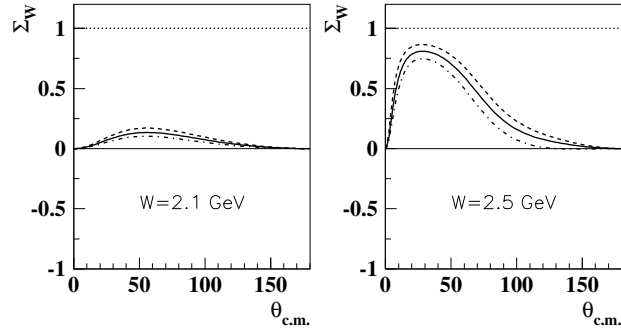


FIG. 6: Polarized beam asymmetries for  $n \rightarrow K^+ \pi^0$  with  $\pi^0$  of negative parity at  $W = 2.1$  and  $2.5$  GeV in the Born approximation limit. The notations are the same as Fig. 5.

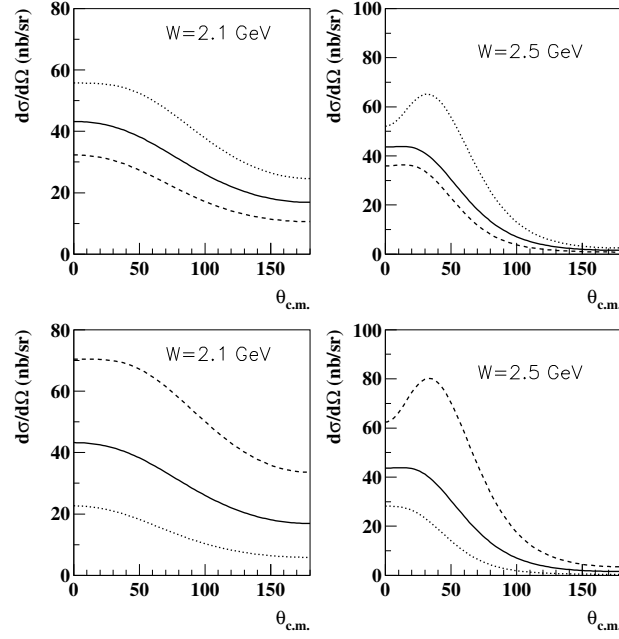


FIG. 7: Differential cross sections for  $\pi^+ p \rightarrow \pi^+ p$  of  $l=2^+$  at  $W = 2.1$  and  $2.5$  GeV with the  $K$  exchange. The solid curves are results in the Born limit, while the dashed and dotted curves denote results with the  $K$  exchange included with different phases:  $(g_{\pi N K}; \delta) = (-2.8; 3.71)$  (dashed curves in the upper two figures),  $(+2.8; 3.71)$  (dotted curves in the upper two figures),  $(-2.8; 3.71)$  (dashed curves in the lower two figures), and  $(+2.8; 3.71)$  (dotted curves in the lower two figures).

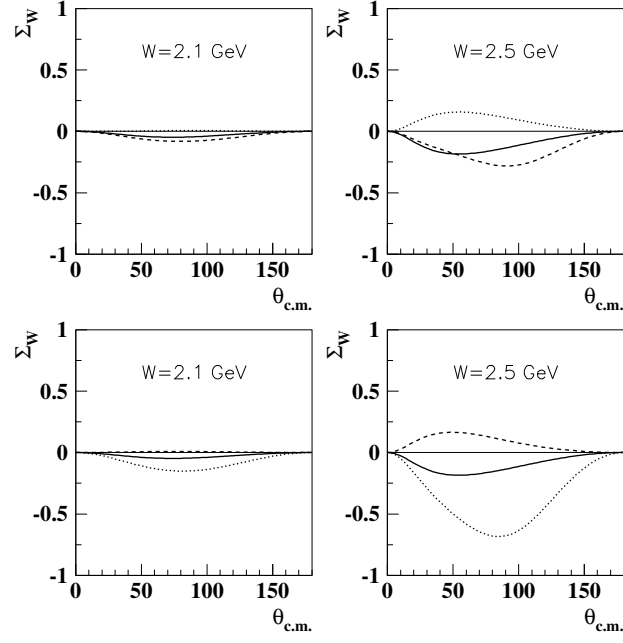


FIG. 8: Polarized beam asymmetries for  $\pi^+$  of  $1=2^+$  at  $W = 2.1$  and  $2.5$  GeV with the  $K$  exchange. The notations are the same as Fig. 7.

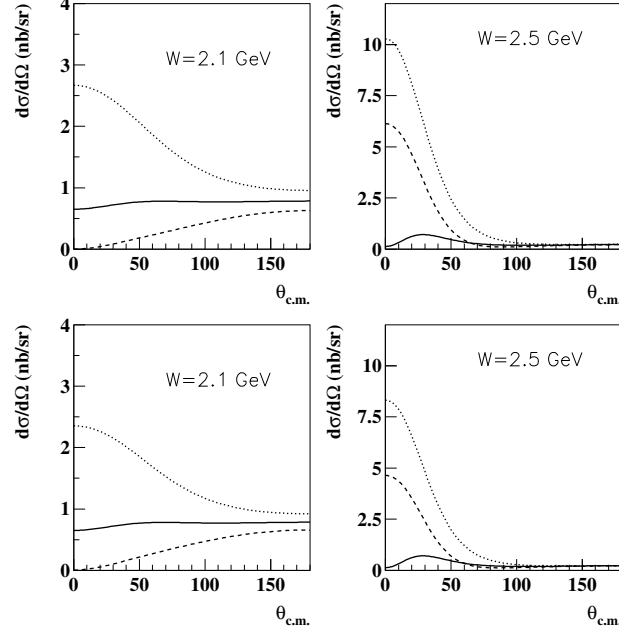


FIG. 9: Differential cross sections for  $\pi^+ \pi^-$  of  $l=2$  at  $W = 2.1$  and  $2.5$  GeV with the  $K$  exchange. The solid curves are results in the Born limit, while the dashed and dotted curves denote results with the  $K$  exchange included with different phases:  $(g_{NK}; \delta) = (0.61; 0.371)$  (dashed curves in the upper two figures),  $(+0.61; +0.371)$  (dotted curves in the upper two figures),  $(-0.61; +0.371)$  (dashed curves in the lower two figures), and  $(+0.61; -0.371)$  (dotted curves in the lower two figures).

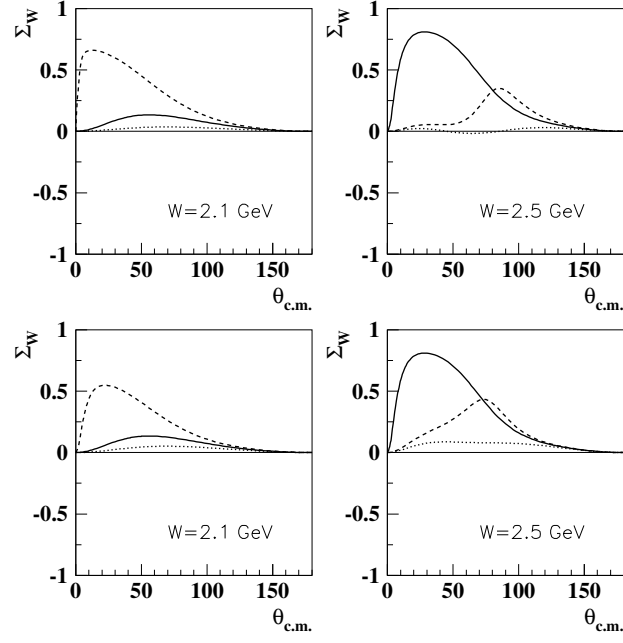


FIG. 10: Polarized beam asymmetries for  $\pi^+$  of  $l=2$  at  $W = 2.1$  and  $2.5$  GeV with the  $K$  exchange. The notations are the same as Fig. 9.